Regular Article

Morphological stability diagram for slowly and rapidly solidifying binary systems

Peter K. Galenko[1,2,a] and Denis A. Danilov[3]

[1] Friedrich-Schiller-Universität-Jena, Faculty of Physics and Astronomy, Otto Schott
Institute of Materials Research, 07743 Jena, Germany
[2] Ural Federal University, Department of Theoretical and Mathematical Physics,
Laboratory of Multi-Scale Mathematical Modeling, 620000 Ekaterinburg, Russia
[3] Udmurt State University, Physical Faculty, 426034 Izhevsk, Russia

Abstract. A linear morphological stability of the solid-liquid interface
is analyzed for a binary alloy in the limit of low and high crystal growth
velocities. Using the result of this analysis, a diagram of morphologies is
derived for a whole range of solidification rates with indicating critical
growth velocities for the transitions planar front ⇔ cellular/dendritic
structure. It is specially noted that the speed of solute diffusion in
the bulk liquid limits the absolute chemical stability velocity from the
high-rate transition cells/dendrites ⇒ planar front.

1 Introduction

Originating of two-phase mushy zone, as a heterogeneous zone of phase transition
between liquid and solid [1,2], occurs as a response of crystallizing liquer/solution/
melt on the existing undercooling for the fastest decrease of this undercooling (see Fig. 1).
Indeed, an intensive atoms attachment to the solid-liquid interface leads to the fast
decrease in the interface undercooling with the formation of crystalline ensemble of cel-
lular or dendritic morphology (see Refs. [4–6] and references therein). In appearance of
such morphologies a key role plays an establishing balance between destabilizing and
stabilizing forces which are competing at the interface leading it to the planar or cel-
lular/dendritic form. Therefore, the originating and development of two-phase mushy
zone are going through the stages of front perturbation on the microscopic spatial level
and formation of mesoscopic structures of cellular-dendritic morphology.

In the present work, we consider linear morphological stability of solidification
front for definition of its morphology for a given growth velocity. This problem takes
its origination from the classical works of Mullins and Secerka [7,8] as well as from
the works of Coriell et al. [9–12]. Later on, this morphological analysis has been
extended to the non-linear range by Davis [13] and generalized to the region of large
growth velocity by Trivedi and Kurz [14–16]. Extended analysis of morphological sta-
bility to the case of local non-equilibrium solidification [17] was necessary to explain
experimental results on crystallization of liquids undercooled up to $400-500\,\mathrm{K}$ and
solidifying with the velocities $1-100\,\mathrm{m/s}$ [18]. Therefore, we present analysis which

---

[a] e-mail: peter.galenko@uni-jena.de
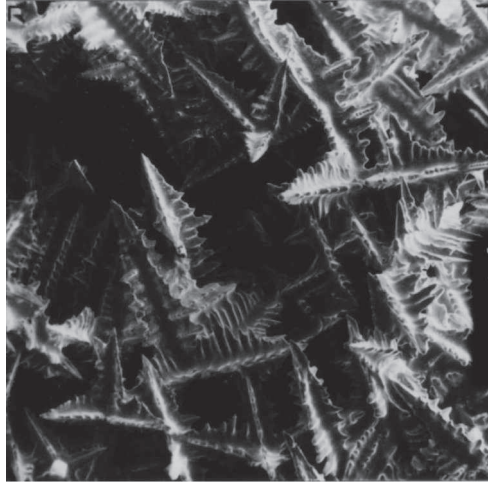
Fig. 1. Dendritic structure within the two-phase mushy zone. This structure has been obtained by decantation of a residual interdendritic melt upon primary solidification of Pb-Sn alloy's droplets [3].

allows us to construct the diagram of morphological stability from very small velocity of crystals growing at the near equilibrium conditions up to the high velocity at which diffusionless (chemically partitionless) solidification may occur.

2 Criterion of the morphological stability

When a harmonic perturbation with the wavelength λ and the corresponding frequency

$$\omega = 2\pi/\lambda \tag{1}$$

is applied to a moving planar interface, the resulting criterion of its marginal stability is given by [17]

$$\Gamma\omega^2 + K_L G_L \xi_L + K_S G_S \xi_S - m_v G_C \xi_C = 0, \qquad V < V_D,$$

$$\Gamma\omega^2 + K_L G_L \xi_L + K_S G_S \xi_S = 0, \qquad V \geq V_D, \tag{2}$$

where indices "L" and "S" are related to the liquid or solid, respectively, G is the thermal gradient, K is the thermal conductivity, V the velocity of the interface, V_D is the solute diffusion speed in bulk liquid, Γ is the Gibbs-Thomson coefficient related to the capillary of the perturbed interface, and m_v is the velocity dependent slope of the liquidus line (so-called "nonequilibrium liquidus in the kinetic diagram of a phase state"). The stability functions ξ in equation (2) are described by

$$\xi_L = \frac{\omega_L - V/a_L}{K_L \omega_L + K_S \omega_S}, \tag{3}$$

$$\xi_S = \frac{\omega_S + V/a_S}{K_L \omega_L + K_S \omega_S}, \tag{4}$$

$$\xi_C = \frac{\omega_C - V/[D(1 - V^2/V_D^2)^{1/2}]}{\omega_C - (1 - k_v)V/[D(1 - V^2/V_D^2)^{1/2}]}, \quad V < V_D,$$

$$\xi_C = 0, \qquad V \geq V_D, \tag{5}$$

where a is the thermal diffusivity, D the diffusion constant and k_v is the velocity dependent solute partitioning function related to nonequilibrium redistribution of atoms on the interface. Frequencies ω have the following form

$$\omega_L = \frac{V}{2a_L} + \left[\left(\frac{V}{2a_L}\right)^2 + \omega^2\right]^{1/2}, \tag{6}$$

$$\omega_S = -\frac{V}{2a_S} + \left[\left(\frac{V}{2a_S}\right)^2 + \omega^2\right]^{1/2}, \tag{7}$$

$$\omega_C = \frac{V}{2D(1 - V^2/V_D^2)^{1/2}} + \left[\left(\frac{V}{2D(1 - V^2/V_D^2)^{1/2}}\right)^2 + \omega^2\right]^{1/2}. \tag{8}$$

In the local equilibrium limit, $V_D \to \infty$, criterion (2) together with equations (3)–(8) transforms into the criterion of marginal stability of Trivedi and Kurz [14]. The introduction of the finite diffusion speed, V_D, into the model leads to the principal result, which is related to the transition to diffusionless (chemically partitionless) solidification. It can be shown using analytical solution for the atomic redistribution around the interface. Indeed, one can obtain two solutions from the only diffusion equation. These describe two different regimes: regime with atomic diffusion at $V < V_D$ and regime with the absence of atomic diffusion at $V \geq V_D$. Particularly, around the perturbed interface, the field of solute concentration is given by [17]

$$C - C_\infty = \frac{G_C D(1 - V^2/V_D^2)}{V}\left[1 - \exp\left(-\frac{Vz}{D(1 - V^2/V_D^2)}\right)\right]$$

$$+ (b - G_C)\delta(t)\sin(\omega x)\exp\left(-\frac{\omega_C z}{(1 - V^2/V_D^2)^{1/2}}\right), \quad V < V_D,$$

$$C - C_\infty = 0, \qquad V \geq V_D, \tag{9}$$

where C_∞ is the nominal (initial) concentration of a binary system which is considered as far-field concentration. Solution (9) shows that with the finite interface velocity $V \geq V_D$, the solute diffusion ahead of the rapid interface is absent. From this it follows that the destabilizing contribution due to concentration gradient G_C in equation (2) is absent at $V \geq V_D$. In such a case, the balance for morphological stability is defined by the relation of the stabilizing force $\Gamma\omega^2$, due to surface energy, and the contribution $K_L G_L \xi_L + K_S G_S \xi_S$ of temperature gradients, $G_L > 0$ and $G_S > 0$, which are positive in the case of directional solidification.

3 Analysis of the stability function

We are interested in the analysis of the concurrence of contribution of the surface energy and destabilizing concentration gradient which is true for $V < V_D$. Therefore, consider the first equation from the criterion (2). For this equation, one can introduce the following stability function (see, for details, Ref. [12]):

$$S(\omega^2) = -\Gamma\omega^2 - K_L G_L \xi_L - K_S G_S \xi_S + mG_C \xi_C. \tag{10}$$

Taking the stability functions from equations (3) and (4) we assume equal coefficients of thermal diffusivity and of thermal conductivity in both phases, i.e., $a_L = a_S = a$

and $K_L = K_S = K_T$. Then we get

$$K_L G_L \xi_L + K_S G_S \xi_S = \frac{G_L + G_S}{2} + \frac{G_S - G_L}{2} \frac{V}{2a} \frac{1}{\sqrt{(V/2a)^2 + \omega^2}}. \quad (11)$$

As a result, the function (10) can be re-written as

$$S(\omega^2) = -\Gamma \omega^2 - \frac{G_L + G_S}{2} - \frac{G_S - G_L}{2} \frac{V}{2a} \frac{1}{\sqrt{(V/2a)^2 + \omega^2}} + m G_C \xi_C(\omega^2). \quad (12)$$

This function has two limiting cases: $\omega^2 = 0$ and $\omega^2 \to \infty$. First, at $\omega^2 = 0$ one has $\xi_C = 0$, and for the positive temperature gradients, $G_L > 0$ and $G_S > 0$, we have from equation (12) the following function

$$S(\omega^2) = -\frac{G_L + G_S}{2} - \frac{G_S - G_L}{2} < 0. \quad (13)$$

Second, at $\omega^2 \to \infty$, one gets from equation (12) that $S(\omega^2) \to -\infty$.

Now let us analyze extremal points of the function $S(\omega^2)$ given by equation (12). With this aim we write the derivative $\partial S(\omega^2)/\partial \omega^2$ as follows

$$\frac{\partial S(\omega^2)}{\partial \omega^2} = -\Gamma + \frac{G_S - G_L}{2} \frac{V}{2a} \frac{1/2}{\left((V/2a)^2 + \omega^2\right)^{3/2}}$$

$$+ \frac{m G_C}{2} \frac{1}{\left(\left(V/\left(2D\sqrt{1 - V^2/V_D^2}\right)\right)^2 + \omega^2\right)^{1/2}}$$

$$\times \frac{kV/\left(D\sqrt{1 - V^2/V_D^2}\right)}{\left(\omega_C - (1 - k)V/\left(D\sqrt{1 - V^2/V_D^2}\right)\right)^2}. \quad (14)$$

From this derivative one can find both asymptotic regimes for rapid solidification and slow solidification.

3.1 The first asymptotic: a case of rapid solidification

It can be seen from equation (14), that the derivative $\partial S(\omega^2)/\partial \omega^2$ is a monotonically diminishing function of ω^2. Accordingly, if $\partial S(\omega^2)/\partial \omega^2 < 0$ at $\omega^2 = 0$, then we get $\partial S(\omega^2)/\partial \omega^2 < 0$ for any ω^2. In such a case, the function $S(\omega^2)$ has not extremal points and it is the negative function, $S(\omega^2) < 0$, for any ω^2 in a positive temperature gradient [see Eq. (13)]. Thus, for this case, the planar interface is morphologically stable.

For the zero frequency, i.e., $\omega^2 = 0$, we get the following condition

$$\frac{\partial S(\omega^2)}{\partial \omega^2} = -\Gamma + \frac{G_S - G_L}{4} \left(\frac{2a}{V}\right)^2 + \frac{m_v G_C D^2 \left(1 - V^2/V_D^2\right)}{k_v V^2} < 0. \quad (15)$$

Omitting the terms with temperature gradients, one can get the stability condition in the following form

$$\Gamma > \frac{m_v G_C D^2 \left(1 - V^2/V_D^2\right)}{k_v V^2}. \quad (16)$$

From this it follows that the solidification planar front is stable if the contribution from the interfacial energy (proportional to Γ) is greater than the destabilizing contribution (proportional to the concentration gradient G_C).

Now, taking into account expression for the concentration gradient G_C at the unperturbed interface [19]

$$G_C = -\frac{(1-k_v)VC_\infty}{k_v D(1-V^2/V_D^2)}, \qquad V < V_D,$$

$$G_C = 0, \qquad V \geq V_D, \tag{17}$$

and using equation (16), one can obtain the following inequality

$$\frac{k_v^2 \Gamma}{m_v(k_v-1)C_\infty} > \frac{D}{V}. \tag{18}$$

This stability condition has the following meaning [20]. As soon as the characteristic diffusion length D/V becomes smaller than the characteristic scale $k_v^2\Gamma/(m_v(k_v-1)C_\infty)$ of interfacial capillary, the planar interface becomes morphologically stable in rapid solidification regime.

The balance between the stabilizing and destabilizing actions [see Eq. (16)] or equality of the two lengths [see Eq. (18)] can be re-written in the following convenient form

$$V_A = \frac{m_v D(k_v-1)C_\infty}{\Gamma k_v^2} \equiv \frac{D\Delta T_v}{k_v \Gamma} < V_D, \tag{19}$$

where

$$\Delta T_v = m_v \frac{k_v-1}{k_v} C_\infty$$

is the velocity dependent interval of solidification (in the kinetic phase diagram). This is the velocity V_A for absolute chemical stability above which the planar interface becomes stable. The form of equation (19) coincides with the expression given for the case of local equilibrium solute diffusion transport at $V_D \to \infty$ [14]. However, a final form of the function $V_A(C_\infty)$ is defined by the functions of solute partitioning, k_v, and the slope, m_v, of liquidus line in the kinetic phase diagram. The behavior of theses functions is rather different for the cases of local equilibrium and local non-equilibrium solute diffusion [17,19,21,22].

3.2 The second asymptotic: a case of slow solidification

To predict condition of stability for the slowly moving planar interface, we consider small solidification velocity. With this aim, one can neglect quadratic terms by velocity V and use the expression $G_S - G_L \sim V$ in equation (14). Also, for the slow-rate solidification regime, one can assume that the velocity dependent functions k_v and m_v merely have their own equilibrium constants k_e and m_e, respectively. Therefore, equation for extrema of the function $S(\omega^2)$ is described by

$$\frac{\partial S(\omega^2)}{\partial \omega^2} = -\Gamma + \frac{mG_C}{2}\frac{1}{\sqrt{(V/2D)^2+\omega^2}}\frac{k_e V/D}{\left(\omega_C-(1-k_e)V/D\right)^2} = 0, \tag{20}$$

where the frequency ω_C is given by (see Eq. (8) with neglecting quadratic terms by velocity V)

$$\omega_C = \frac{V}{2D} + \sqrt{\left(\frac{V}{2D}\right)^2 + \omega^2}. \tag{21}$$

Using the new variable r defined by

$$r^2 = \left(1 + (2D\omega/V)^2\right)^{1/2}, \tag{22}$$

equation (20) takes the following form

$$-\Gamma + \frac{mG_C}{2} \cdot \frac{1}{(V/2D)r^2} \cdot \frac{k_e V/D}{\left((V/2D)(r^2 + 2k_e - 1)\right)^2} = 0. \tag{23}$$

This equation can be easily re-written as follows

$$r^3 + (2k_e - 1)r - (2k_e/A^{1/2}) = 0, \tag{24}$$

where the parameter A is given by

$$A = \frac{k_e \Gamma V^2}{m_e G_C D^2}. \tag{25}$$

Cubic polynomial (24) has been analyzed in details by Sekerka and Coriell in references [9,10]. In particular, defining $\mathcal{G} = \overline{G}/(m_e G_C)$, where $\overline{G} = (G_L + G_S)/2$ is the weighted temperature gradient, and using equation (10), the following relationship at the onset of instability is found [9]:

$$\mathcal{G} = 1 - \frac{3}{2}rA^{1/2} + \frac{A}{4k_e}[1 - (1 - 2k_e)r^2], \tag{26}$$

where r is the one real root greater than unity of equation (24). For slow solidification, the parameter A given by equation (25) is small compared to unity. Consequently, equation (26) leads to the following criterion [11]:

$$\mathcal{G} = 1, \tag{27}$$

which is known as the modified constitutional supercooling criterion [12] equals to

$$\overline{G} = m_e G_C \equiv mC_\infty \frac{k_e - 1}{k_e} \frac{V}{D}, \tag{28}$$

where equation (17) has been taken into account for small velocity, $V << V_D$.

Equation (28) shows that the liquid ahead of the interface is constitutionally supercooled if $\overline{G} < m_e G_C$ that is leading to morphological instability of the planar solidification front. Neglecting the thermal gradient in solid and using $\overline{G} = G_L$, one can get from equation (28) the constitutional supercooling criterion in its classical form given by Ivantsov and Tiller et al. [23,24].

4 Model with the deviations from local equilibrium at the interface and in solute diffusion field

For computation of the morphological stability diagram we assume that characteristic size of pattern upon instability of the planar solidification interface is defined by the marginal stability hypothesis given by the analysis of Langer and Müller-Krumbhaar [25]. Following this hypothesis, the size R of pattern is equal to the critical wavelength

λ of equation (1). Therefore, using, criterion (2), for a given velocity $V < V_D$ and temperature gradients G_L and G_S, the pattern size R is defined by

$$R = \left(\frac{\Gamma/\sigma}{m_v G_C \xi_c - \frac{1}{2}(G_L \xi_L + G_S \xi_S)} \right)^{1/2}, \tag{29}$$

where $\sigma = (4\pi^2)^{-1}$ is a parameter of marginal stability giving relation between R and a wavelength of interfacial perturbation.

For the case of local non-equilibrium solute diffusion, the gradient G_C is defined as follows [26]

$$G_C = -\frac{V}{D} \frac{(1 - k_v)C_\infty}{(1 - V^2/V_D^2)(1 - (1 - k_v)\mathrm{Iv}(P_C))}, \qquad V > V_D,$$

$$G_C = 0, \qquad V \geq V_D, \tag{30}$$

where $P_C = VR/2D$ is the solutal Peclet number. The Ivantsov-function $\mathrm{Iv}(P)$ is defined by:

$$\mathrm{Iv}(P) = (\pi P)^{1/2} \exp(P)\mathrm{erfc}(P^{1/2}), \qquad \text{for 2D},$$

$$\mathrm{Iv}(P) = P \exp(P)\mathrm{E_i}(P), \qquad \text{for 3D}, \tag{31}$$

where $\mathrm{E_i}(P) = \int_P^\infty s^{-1} \exp(-s)ds$ is the exponential integral function. The stability functions ξ can be obtained from equations (3)–(5) as follows [17]

$$\xi_L = 1 - \frac{1}{\left(1 + \dfrac{1}{\sigma P_T^2}\right)^{1/2}}, \tag{32}$$

$$\xi_S = 1 + \frac{1}{\left(1 + \dfrac{1}{\sigma P_T^2}\right)^{1/2}}, \tag{33}$$

$$\xi_C = 1 + \frac{2k_v}{1 - 2k_v - \left(1 + \dfrac{1 - V^2/V_D^2}{\sigma P_C^2}\right)^{1/2}}, \quad V < V_D,$$

$$\xi_C = 0, \qquad V \geq V_D, \tag{34}$$

where $P_T = VR/2a$ is the thermal Peclet number.

The slope m_v of the nonequilibrium liquidus is described by [21]:

$$m_v = \frac{m_e}{1 - k_e} \left\{ 1 - k_v + \ln\left(\frac{k_v}{k_e}\right) + (1 - k_v)^2 \frac{V}{V_D} \right\}, \quad V < V_D,$$

$$m_v = \frac{m_e \ln k_e}{k_e - 1}, \qquad V \geq V_D. \tag{35}$$

The solute distribution function k_v at the interface defines the solute trapping and it is described by [27]:

$$k_v = \frac{(1 - V^2/V_D^2)[k_e + (1 - k_e)C_\infty] + V/V_{DI}}{1 - V^2/V_D^2 + V/V_{DI}}, V < V_D,$$

Table 1. Physical parameters of Si–Sn alloy used in calculations of the morphological stability diagrams.

Parameter	Notation	Dimension	Values	Reference
Thermal conductivity	K_L	W/K/m	140	[30]
Heat capacity	c_p	J/K/m^3	2.5×10^6	[30]
Diffusion coefficient	D	m^2/s	2.5×10^{-8}	[31]
Partition coefficient	k_e	—	0.016	[31]
Liquidus slope	m_e	K/at.%	-4.6	[31]
Gibbs-Thomson coefficient	Γ	K m	1.3×10^{-7}	[31]
Interface diffusion speed	V_{DI}	m/s	17	[31]
Diffusion speed in bulk liquid	V_D	m/s	17.5	[17]

$$k_v = 1, \qquad V \geq V_D, \tag{36}$$

where V_{DI} is the interfacial diffusion speed [28,29] which is usually assumed to be $V_{DI} < V_D$.

As a result, equations (29)–(36) generalize the model of Kurz, Giovanola, and Trivedi (KGT-model) [15] for the case of deviation from local equilibrium in bulk liquid (i.e., in the solute diffusion field). The KGT-model itself directly follows from equations (30)–(36) in the limits $V_D \rightarrow \infty$.

5 Morphological stability diagram

For the further analysis, we assume that (i) the solidification proceeds in the positive temperature gradient in the liquid and one can neglect the gradient in the solid, so that $G_L > 0$ and $G_S = 0$ and (ii) all calculations will be made for material parameters of Si–Sn alloy summarized in Table 1.

5.1 Critical values of parameters

With a given velocity V and for various gradients G_L, equation (29) may have the only solution, two solutions, or no any solutions. These three situations are shown in Figure 2 using the dashed-dotted line, dashed line, and dotted line, respectively. If G_L is smaller than some critical value $G^*(V)$, then equation (29) has two roots the minima of which give the selected size of crystalline microstructure. As the temperature gradient increases up to the critical value $G^*(V)$, equation (29) has the only root which gives the maximal characteristic size of the microstructure at a given interface velocity V. Further increasing the gradient G_L leads to the absence of any solution for equation (29) that gives a stability of the planar interface with $R \rightarrow \infty$. Thus, a curve for the critical temperature gradient $G^*(V)$ defines V and G_L at which the transition from planar front to cells and dendrites or *vice versa* may occur in a binary alloy.
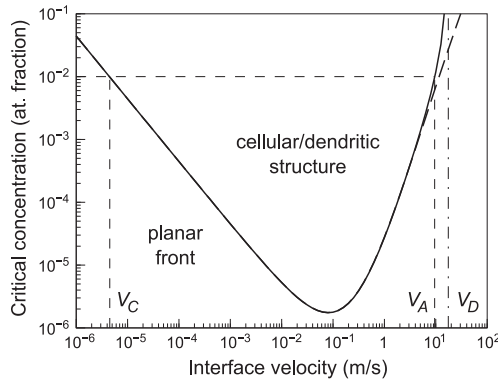
5.2 The complete diagram of morphology

Figure 3 presents morphological stability diagram which is known as "nose-like diagram of interfacial stability" [32,33]. The diagram shows regions of planar front stability and of cells/dendrites existence for given nominal concentration and interface
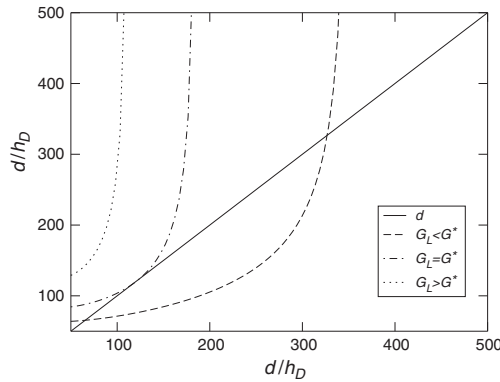
Fig. 2. Dependence of left hand side (solid line) and right hand side (dotted, dashed and dashed-dotted) of equation (29) on characteristic size R of microstructure. The curves are plotted for given velocity V and various gradients G_L. The size R is scaled by the diffusion length $h_D = D/V_D$.
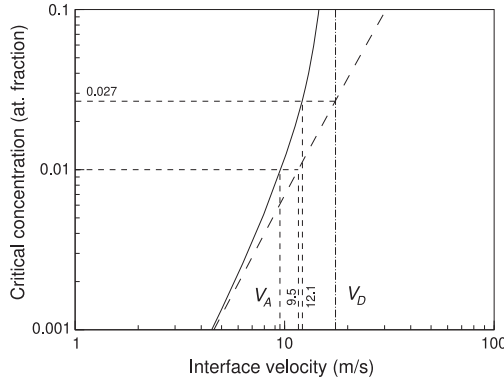

Fig. 3. The complete morphological stability diagram in a form of critical concentration, $C_\infty(V)$, above which planar interface is unstable (solid line) for a given temperature gradient $G_L = 10^5\,\text{K/m}$. The limiting velocity V_C is given by equation (28) and the limiting velocity V_A is given by equations (19), (35) and (36). Dashed-dotted line, $V = V_D$, represents the limiting velocity for the absolute interface stability.

velocity V. The most important issue that the diagram predicts critical value for the transitions between growing structures in steady state crystalline solidification obtained by the constitutional criterion (28) at small V and absolute chemical stability condition (19), (35) and (36) given by the high V-limit. In addition to the structure diagram calculated in reference [17] the diagram in Figure 3 represents the whole range of the front velocities from its low to high values at which morphological transitions may occur at the corresponding values of the critical concentration.

5.3 High velocity limit and dependence on temperature gradient

The high V-limit given in the complete diagram principally differs from the previously obtained in references [32]. Indeed, as Figure 4 shows (which is zoom of Fig. 3 for the region of high growth velocity), the model with the deviation from local equilibrium only at the interface predicts gradual increasing of concentration with no sensetive to the bulk diffusion speed (dashed line). By contrast, the model with deviation

Fig. 4. A part of the morphological stability diagram for high solidification rates given by equations (19), (35) and (36).
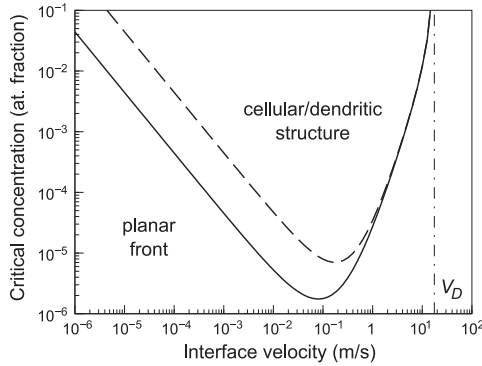
Fig. 5. Dependence of the morphological stability from the temperature gradient as predicted by equations (19), (35) and (36). The curves are computed for various temperature gradients: solid line is given by $G_L = 10^5$ K/m, and dashed line is given by $G_L = 10^6$ K/m. Dashed-dotted line, $V = V_D$, represents the limiting velocity for the absolute interface stability.

from local equilibrium at the interface and in bulk diffusion field is limited by the diffusion speed in bulk liquid and one gets $V_A < V_D$. As a result the curve of critical concentration (solid line in Fig. 4) essentially deviates from that one given by the model with the deviation from local equilibrium only at the interface (i.e. from the dashed line in Fig. 4). Such deviation around $V = V_A$ gradually increases and leads to essential difference inpredictions of the growth kinetics of dendrites [18]. One can note that for the diffusion coefficient D, equilibrium partition coefficient k_e and the liquidus line slope m_e we have used in calculations their constant values independent on temperature and concentration (see Tab. 1). In a wide range of undercooling and for a dilute and concentrated alloys these material parameters should be taken as functions of temperature and concentration that is, of course, may correct the morphological diagram shown in Figures 3 and 5.

Finally, one has to note that the temperature gradient G_L mainly influences the critical concentration for the morphology transition at small growth velocity. Figure 5 shows that the increase in $G_L > 0$ leads to the increase in the region for the planar front stability at small velocity V. This fact follows from the criterion of constitutional

undercooling (28) if it can be rewritten in the form

$$C_\infty = \frac{k_e}{m_e(k_e - 1)} \cdot \frac{DG_L}{2V}, \quad \text{where } \overline{G} = G_L/2, \tag{37}$$

which predicts that the nominal concentration C_∞ should be increased as the temperature gradient G_L increases for a given interface velocity V. By contrast, the high velocity limit does not strongly depend on the gradient G_L. It appears due to definition of absolute chemical stability: the criterion (19) is the result of competition and balance of the capillary length and solute diffusion length that does not depend of the imposed temperature gradient directly.

6 Conclusions

Using the criterion of marginal stability we found the conditions of constitutional undercooling, which acts at small solidification rates, and the absolute chemical stability as a result of the competition between contributions of surface energy and destabilizing concentration gradient. These conditions are related to general solidification regimes existing at very small and very high solid-liquid interface velocity, which occur under deviation from local equilibrium at the interface and in the diffusion profile in bulk liquid. As well as these conditions present in asymptotic cases of the complete regimes obtained from the diagram of morphologies computed using the formulated model of dendritic/cellular growth.

The constructed morphology diagram predicts critical values of concentration and interface velocity dividing the region of planar solidification front stability and the region of cellular/dendritic structures growing in a positive temperature gradient during slow, intermediate and rapid directional solidification of binary alloys. Combinations of the full diagram of structures and dynamic conditions of the existence of stationary or non-stationary modes of solidification complement the interpretation of experimental results [34].

Author contribution statement

All authors contributed equally to the present research article.

References

1. V.T. Borisov, *Theory of two-phase mushy zone of metallic ingot* (Metallurgia, Moscow, 1987)

2. V.A. Zhuravlev, *Solidification and crystallization of alloys with hetero-trasformations* (Regular and Chaotic Dynamics, Izhevsk, 2006)
3. V.T. Borisov, Yu.E. Matveev, Fizika Metallov i Metallovedenie **13**, 465 (1962)
4. R. Trivedi, W. Kurz, Int. Mater. Rev. **39**, 49 (1994)
5. W. Kurz, D.J. Fisher, R. Trivedi, Int. Mater. Rev. **64**, 311 (2019)
6. P.K. Galenko, D.V. Alexandrov, Philos. Trans. R. Soc. A **376**, 20170210 (2018)
7. W.W. Mullins, R.F. Sekerka, J. Appl. Phys. **34**, 323 (1963)
8. W.W. Mullins, R.F. Sekerka, J. Appl. Phys. **35**, 444 (1964)
9. R.F. Sekerka, J. Appl. Phys. **36**, 264 (1965)
10. S.R. Coriell, R.F. Sekerka, in *Rapid solidification processing II*, edited by R. Mehrabian, B.H. Kear, M. Cohen (Claitor's, Baton Rouge, Louisiana, 1980), p. 35
11. S.R. Coriell, G.B. McFadden, R.F. Sekerka, Annu. Rev. Mater. Sci. **15**, 119 (1985)
12. S.R. Coriell, G.B. McFadden, in *Handbook of crystal growth*, edited by D.T.J. Hurl (Elsevier, Amsterdam, 1993), Vol. 1a, p. 785
13. S.H. Davis, *Theory of solidification* (Cambridge University Press, Cambridge, UK, 2001)
14. R. Trivedi, W. Kurz, Acta Metall. **34**, 1663 (1986)
15. W. Kurz, B. Giovanola, R. Trivedi, Acta Metall. **34**, 823 (1986)
16. W. Kurz. D.J. Fisher, *Fundamentals of solidification*, 3rd edn. (Trans Tech Publications, Aedermannsdorf, 1992)
17. P.K. Galenko, D.A. Danilov, Phys. Rev. E **69**, 051608 (2004)
18. D.M. Herlach, P.K. Galenko, D. Holland-Moritz, *Metastable solids from undercooled melts*, (Elsevier, Amsterdam, 2007)
19. P.K. Galenko, D.A. Danilov, J. Cryst. Growth **216**, 512 (2000)
20. W.J. Boettinger, S.R. Coriell, R.F. Sekerka, Mater. Sci. Eng. A **65**, 27 (1984)
21. P. Galenko, Phys. Rev. B **65**, 144103 (2002)
22. P.K. Galenko, Mater. Sci. Eng. A **375-377**, 493 (2004)
23. G.P. Ivantsov, Dokl. Akad. Nauk SSSR **81**, 179 (1951)
24. W.A. Tiller, K.A. Jackson, J.W. Rutter, B. Chalmers, Acta Metall. **428**, 1 (1953)
25. J.S. Langer, H. Müller-Krumbhaar, Acta Metall. **26**, 1681 (1978)
26. P.K. Galenko, D.A. Danilov, Phys. Lett. A **235**, 271 (1997)
27. P. Galenko, Phys. Rev. E **76**, 031606 (2007)
28. M.J. Aziz, T. Kaplan, Acta Metall. **36**, 2335 (1988)
29. M.J. Aziz, J. Appl. Phys. **53**, 1158 (1982)
30. D.E. Hoglund, M.O. Thompson, M.J. Aziz, Phys. Rev. B **58**, 189 (1998)
31. D.E. Hoglund, M.J. Aziz, Mater. Res. Soc. Symp. Proc. **205**, 325 (1992)
32. D.E. Hoglund, M.J. Aziz, S.R. Stiffler, M.O. Thompson, J.Y. Tsao, P.S. Peercy, J. Cryst. Growth **109**, 107 (1991)
33. H. Biloni, W.J. Boettinger, Solidification, in *Physical metallurgy*, edited by R.W. Cahn, P. Haasen, (Elsevier Science Publishers, Amsterdam, 1996), Vol. I, Chap. 8, pp. 669–842
34. K. Reuther, P.K. Galenko, M. Rettenmayr, J. Cryst. Growth **506**, 55 (2019)